Thermal desorption of C_6H_6 from surfaces of astrophysical relevance

J. D. Thrower,[1,a)] M. P. Collings,[1] F. J. M. Rutten,[2] and M. R. S. McCoustra[1,b)]
[1]*School of Engineering and Physical Sciences, Heriot-Watt University, Edinburgh EH14 4AS, United Kingdom*
[2]*School of Pharmacy and iEPSAM, Keele University, Keele ST5 5BG, United Kingdom*

(Received 23 July 2009; accepted 4 November 2009; published online 29 December 2009)

The thermal desorption of C_6H_6 from two astrophysically relevant surfaces has been studied using temperature programmed desorption. Desorption from an amorphous SiO_2 substrate was used as a mimic for bare interstellar grains, while multilayer films of amorphous solid water (ASW) were used to study the adsorption of C_6H_6 on grains surrounded by H_2O dominated icy mantles. Kinetic parameters were obtained through a combination of kinetic modeling, leading edge analysis, and by considering a distribution of binding sites on the substrate. The latter is shown to have a significant impact on the desorption of small exposures of C_6H_6 from the amorphous SiO_2 substrate. In the case of adsorption on ASW, dewetting behavior and fractional order desorption at low coverage strongly suggest the formation of islands of C_6H_6 on the H_2O surface. The astrophysical implications of these observations are briefly outlined. © *2009 American Institute of Physics*.
[doi:10.1063/1.3267634]

I. INTRODUCTION

The interactions of aromatic molecules such as benzene (C_6H_6) with other molecules are made more complex by the presence of the conjugated aromatic π system. Indeed, aromatic ring systems such as C_6H_6 have been shown to form relatively strong hydrogen bonds with water (H_2O) through their aromatic π electron systems.[1,2] Such bonds are believed to have an important biochemical role. The strength of this bond for H_2O–C_6H_6 has been measured experimentally to be 9.4 kJ mol^{-1},[3] compared to the value for the H_2O–H_2O hydrogen bond of 15.1 kJ mol^{-1}.[4] The interaction between the C_6H_6 molecules and $(H_2O)_n$ clusters has been studied by Zwier and co-workers[5–7] using resonance enhanced ionization techniques and resonant ion-dip IR spectroscopy.[8] These studies indicate that in the case of $n=1$ the H_2O is positioned with its axis coincident with the C_6 axis of C_6H_6, about which it is free to rotate. In larger clusters, the additional H_2O molecules are situated away from that which is hydrogen bonded to the C_6H_6 molecule, such that C_6H_6 can be considered to bind to a H_2O surface. In an astrophysical context, polycyclic aromatic hydrocarbons (PAHs) are thought to be present throughout the interstellar medium (ISM) (Ref. 9) and to account for up to 20% of the galactic carbon.[10] The importance of PAHs in various astrophysical environments has resulted in numerous experimental studies which have been reviewed extensively from an astrophysical viewpoint.[11] As well as contributing to observed absorption and emission features, experiments suggest that PAHs may also play a role in the formation of more complex organic species such as alcohols, quinones, and ethers.[12]

The dense ISM is known to contain significant amounts of dust, with evidence suggesting a distribution of grain sizes.[13] The existence of two interstellar dust grain populations consisting of silicate minerals and carbonaceous particles is indicated by the depletion of C and Si atoms from the gas phase, along with interstellar extinction.[14] Infrared absorption features attributable to silicate materials have also been observed in spectra obtained during the Infrared Space Observatory (ISO) mission, see, for example, Ref. 15. In cold dense clouds, many gas phase species condense onto the surfaces of these grains with H_2O, thought to be formed *in situ* on the grain surface,[16] dominating the ice mantle that is formed. PAHs are therefore thought to exist within a H_2O ice matrix under such conditions and the IR spectra of a series of PAHs and the impact of this on the observed IR spectra of interstellar PAHs have been investigated experimentally.[17] In warmer regions, direct interactions between adsorbate molecules and the grain surface are likely to become important. It is therefore desirable to understand at a fundamental level the interactions between PAHs and realistic grain and H_2O ice surfaces. Both the desorption kinetics and ice morphology are of interest to astronomers with recent experimental studies highlighting the importance of the latter on the nonthermal processing of interstellar ice mimics.[18] C_6H_6 provides an experimentally convenient system for studying the interactions between aromatic molecules and different surfaces. C_6H_6 itself has been detected in the protoplanetary nebula CRL-618,[19] although it is thought to exist with significantly lower abundance than larger PAHs since it is readily destroyed by irradiation with UV photons. C_6H_6 is also an important intermediate in the formation of PAHs in circumstellar environments,[20,21] which is thought to be initiated by C_2H_2 polymerization.[22]

In this paper we report temperature programmed desorption (TPD) studies of C_6H_6 adsorbed on both an interstellar grain mimic based on amorphous SiO_2 and on compact amorphous solid water (ASW). The former is used as a

[a)]Current address: Department of Physics and Astronomy, Aarhus University, 8000 Aarhus C, Denmark.
[b)]Author to whom correspondence should be addressed. Electronic mail: m.r.s.mccoustra@hw.ac.uk.

simple model of grains in the silicate mineral class that incorporates some of the morphological features and the gross chemical nature of the grain, without introducing the complexities of the metal atoms existing in real minerals. The adsorption of C_6H_6 on single crystal surfaces has been studied in great detail over many years. Examples include graphite,[23] Pt(111),[24] Pd(111),[25] Cu(111),[26] Ru(001), and Ag(111).[27] The amorphous SiO_2 substrate developed in this work is, as a direct result of our attempt to model complex interstellar grains, far from the "ideal" surfaces of previous work. A full characterization of the nature of this surface is therefore far from straightforward, and beyond the scope of this paper. Nevertheless, it is these non-ideal properties of the substrate that make it an attractive model for interstellar grains. As far as we are aware, there are no studies of C_6H_6 adsorption on silica surfaces under ultrahigh vacuum (UHV) conditions, although the interaction between C_6H_6 and silica gel has been studied under ambient conditions.[28–30] The interaction between C_6H_6 and amorphous H_2O ice surfaces has been studied with vibrational spectroscopy,[31,32] metastable impact electron spectroscopy,[32] time-of-flight secondary ion mass spectrometry,[33] and TPD.[32,33] In particular, reflection-absorption infrared spectroscopy of C_6H_6 codeposited with H_2O revealed a strong downshift of the dangling hydrogen-bond vibration, indicating that C_6H_6 binds to H_2O as a proton acceptor. The thermal desorption studies reported here are generally in good agreement with these previous studies of C_6H_6 adsorption on the H_2O ice surface, although the desorption kinetics are considered in somewhat more detail here, in order to allow comparisons between the two C_6H_6-substrate systems in an astrophysical context.

II. EXPERIMENTAL

The experiments discussed here were conducted in a stainless steel UHV chamber that has been described in detail elsewhere.[34,35] The UHV chamber is pumped by a combination of liquid nitrogen trapped diffusion pumps and a titanium sublimation pump. A base pressure of 1×10^{-10} torr is routinely achieved. A quadrupole mass spectrometer (QMS) is attached to the system and was used for monitoring the residual gas environment within the chamber, and for detecting desorbing species during TPD experiments. Suitable optics and a Fourier transform IR spectrometer are interfaced to the system for acquisition of reflection-absorption infrared (RAIR) spectra using an externally mounted mercury cadmium telluride detector. A molecular beam system, originally designed for producing supersonic molecular beams, was used in these experiments for H_2O deposition. An effusive beam was produced by using a nozzle with a significantly larger orifice (approximately 0.5 mm) than that used previously (approximately 50 μm) to obtain supersonic beams.

The amorphous SiO_2 surface used in these experiments was deposited on a polished stainless steel disk of diameter 10 mm using electron beam evaporation of bulk SiO_2. The deposition was performed in a separate high vacuum chamber using 7 keV electrons. The chamber pressure prior to evaporation was around 4×10^{-7} torr. As this chamber was unbaked, the residual gas environment was dominated by H_2O. It is therefore reasonable to assume the presence of a significant number of silanol groups (OH terminated Si species) on the surface thus formed. Furthermore, exposure of the surface to the ambient environment in order to transfer the substrate to the UHV chamber would further facilitate the formation of silanol groups. The film thickness was monitored by means of a quartz crystal microbalance mounted close the deposition region and was estimated to be 200 nm. Atomic force microscopy (AFM) images of the film have been discussed elsewhere[36] and indicate a uniform coverage across the substrate, with the surface displaying a high degree of roughness. Comparison to interplanetary dust particles has shown that this surface is likely to provide a reasonable representation of interstellar grain surfaces.[36] Polarization-modulation RAIRS under ambient conditions was used to confirm the presence of a thick film of SiO_2. However, this technique is not sensitive to surface species, such as silanol groups, on this surface as they will be randomly oriented as a result of the surface roughness.

Following deposition, the substrate was mounted, using tantalum wires, between two molybdenum rods extending from an oxygen free high conductivity copper mount that was in thermal contact with a liquid nitrogen reservoir. Electrical insulation was provided by a sapphire spacer to allow resistive heating of the substrate. A minimum substrate temperature of approximately 115 K was achieved during these experiments. The substrate was prepared by heating to 500 K for 15 min to remove volatile contaminants before cooling, prior to conducting experiments each day. Although this procedure is unlikely to have been sufficient to remove any residual carbon that may have resulted from decomposition of C_6H_6 on the surface, there were no discernible changes in TPD traces over time. The substrate could therefore be prepared in a reproducible manner prior to each experiment without performing annealing or Ar^+ sputtering cycles which might lead to morphological changes, partial crystallization of the SiO_2 film and loss of silanol groups. Indeed, some degree of carbon contamination is not unrealistic, given that real interstellar grains are likely to be far from clean.

During TPD experiments the substrate was heated linearly at a rate of 0.1 ± 0.02 K s^{-1} and desorbing molecules were detected using a QMS (modified VG Micromass PC300D) with a cross-beam ion source and channeltron detector that was operated in analog mode. The QMS was housed in a stainless steel housing within the main UHV chamber with differential pumping being provided by an ion pump. A 5 mm diameter tube extended from the housing in line with the ion source of the QMS. This provided a geometric line-of-sight between the substrate and QMS, significantly reducing the detection of molecules desorbing from surfaces other than the substrate. The substrate temperature was monitored using a K-type (Chromel-Alumel) thermocouple spot-welded to the edge of the substrate. C_6H_6 and H_2O were detected by their parent ions with masses 78 and 18 m_u, respectively.

UV-Spectroscopy grade C_6H_6 (Fluka) and de-ionized H_2O were purified by repeated freeze-pump-thaw cycles on independent manifolds to eliminate the possibility of cross

contamination. C_6H_6 was deposited onto the substrate by means of background dosing of C_6H_6, with the chamber pressure being monitored by a hot cathode ionization gauge. Doses are reported in Langmuir (1 L=10^{-6} torr s), and were converted to molecular concentrations through application of simple collision theory and an ion gauge sensitivity factor for C_6H_6 of 6 relative to N_2.[37] H_2O was dosed using an effusive beam produced in the molecular beam system attached to the main chamber. The beam was approximately 10 mm in diameter, sufficient to completely cover the substrate, and the source chamber was typically operated at a pressure of 2×10^{-4} mbar. The H_2O flux was determined to be $(3.4\pm1)\times10^{17}$ molecules m^{-2} s^{-1} by comparing TPD traces and RAIR spectra obtained with the use of the beam and background dosing. H_2O was deposited onto the SiO_2 substrate held at <120 K, conditions under which a compact ASW film is known to be formed.[38] Preliminary H_2O TPD experiments (not shown) displayed the characteristic desorption feature at approximately 150 K attributed to the crystallization of ASW,[39,40] providing further evidence for the amorphous nature of the H_2O film formed in these experiments. In all experiments performed on top of an ASW layer, the H_2O surface concentration was approximately 7×10^{16} molecules cm^{-2}. We consider this concentration, corresponding to around 100 layers, to be sufficient to completely cover the SiO_2 surface, with the TPD of H_2O clearly displaying zero-order desorption kinetics, in agreement with our previous studies of thick H_2O films.[39] RAIR spectra (not shown) were consistent with those obtained in previous investigations of ASW (Ref. 40) and multilayer C_6H_6 (Ref. 41) films.

III. RESULTS AND DISCUSSION

A. Adsorption of C_6H_6 on amorphous SiO_2

Experimental TPD traces for the desorption of small exposures of C_6H_6 from the amorphous SiO_2 substrate are shown in Fig. 1. C_6H_6 was deposited with the substrate held at 115 K. At the lowest exposure of 0.1 L used in these experiments, the desorption trace displays a single, broad peak, centered at around 190 K, which will be referred to as peak A. The intensity of this feature increases as the C_6H_6 exposure is increased, and the peak maximum is observed to shift to lower temperature. However, the trailing edge of peak A does not shift with increasing exposure resulting in a tail-like feature that is present for all submonolayer exposures. As the exposure is further increased, a second feature, labeled peak B, begins to emerge at lower temperatures, being centered around 140–150 K. This peak continues to shift to lower temperature, although to a lesser extent than the shift observed for peak A, and displays non-coincident trailing edges. Peak B dominates the desorption traces between exposures of 1 and 2 L, as shown in Fig. 1(b), before a strong feature, peak C, appears at around 145 K. This displays a small shift to lower temperature as the exposure is increased, while at the same time the intensity of peak B is rapidly diminished. Peaks A and B are attributed to desorption from the first two layers of C_6H_6 on the SiO_2 substrate, while peak C is thought to result from desorption from the

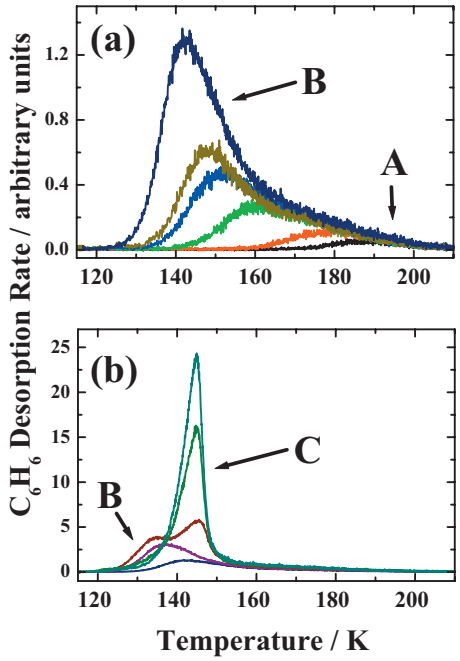

FIG. 1. Experimental TPD traces for the desorption of (a) 0.1, 0.2, 0.5, 0.7, 0.8, and 1 L and (b) 1, 2, 3, 4, and 5 L exposures of C_6H_6 from the amorphous SiO_2 substrate. C_6H_6 was deposited with the substrate held at 115 K. A indicates the high temperature desorption tail, B indicates the desorption of first and second layers, and C indicates the desorption from the first few multilayers. A heating rate of 0.1 ± 0.02 K s^{-1} was used in all cases.

first few multilayers. The addition of further C_6H_6 layers results in a single peak associated with desorption from a thick multilayer film of C_6H_6, which will be discussed subsequently.

Figure 2 shows the TPD yield, obtained by integrating the TPD curve with respect to time, as a function of exposure in molecules per cm^{-2}. Exposures were calculated by application of simple collision theory[42] assuming a sticking probability of unity. It is apparent from Fig. 2 that there is no strong deviation from linearity that would suggest a reduced sticking probability and/or residence time for exposures >0.8 L. This linearity continues to the highest exposure

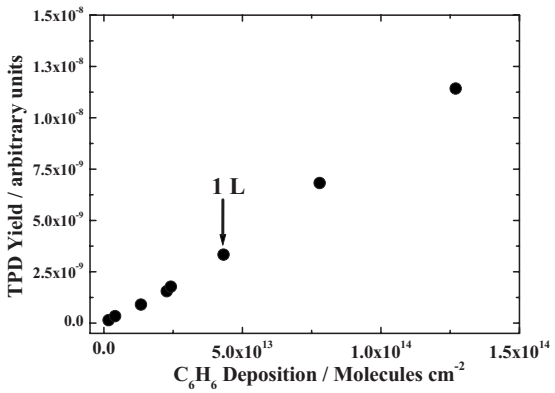

FIG. 2. Uptake curve for C_6H_6 adsorption on amorphous SiO_2 showing the TPD yield as a function of calculated exposure up to that calculated for 3 L. The absence of any significant changes in slope indicates a reasonably constant sticking probability over the submonolayer region. The exposure corresponding to 1 L at which a change in desorption kinetics was observed is indicated.

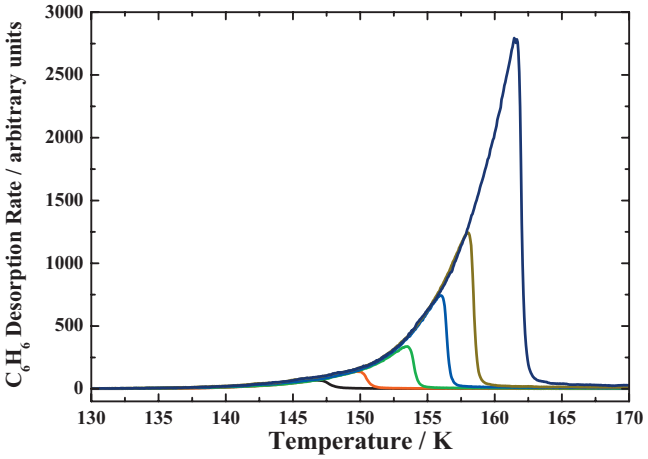

FIG. 3. Experimental TPD traces for the desorption of 10, 20, 50, 100, 200, and 500 L exposures of C_6H_6 from the amorphous SiO_2 substrate. The coincidence of leading edges, characteristic of zero-order desorption kinetics, is clearly displayed. A heating rate of 0.1 ± 0.02 K s^{-1} was used in all cases.

used indicating no significant changes in sticking probability over the full exposure range investigated. We therefore attribute the non-coincidence of trailing edges for the 1 and 2 L peaks, to changes in the desorption kinetics resulting from the formation of a second layer of C_6H_6. As such, peaks A and B are not thought to be separable, with the change in shape resulting from a combination of the population of lower binding energy sites in the first, and the effect of populating sites in the second layer. This will be discussed in more detail later when the low coverage TPD profiles for C_6H_6 desorption from the two substrates are compared. For exposures of greater than 10 L up to the maximum exposure studied (500 L), as shown in Fig. 3, a single peak is visible. The maximum of this peak shifts to higher temperature with increasing exposure. Desorption peaks for all exposures in this regime display coincident leading edges and a very rapid decrease in desorption rate for temperatures above that at which the peak maximum occurs. The nature of this peak indicates that it is due to the desorption of C_6H_6 from a thick multilayer film.

It is clear from these desorption traces that the desorption of small amounts of C_6H_6 from the amorphous SiO_2 surface is complicated, and far from the ideal first order desorption that might occur for species that interact weakly with each other from flat, single crystal surfaces. It is important to recognize that in the present case, the observed desorption kinetics are likely to arise as a result of both substrate and adsorbate effects. The desorption of C_6H_6 at low coverages displays an extremely broad feature, centered at high temperature. Such behavior can be interpreted in terms of a distribution of adsorption sites, which is reasonable given the rough, amorphous nature of the SiO_2 surface revealed by AFM.[36] Previous experiments conducted using an uncoated stainless steel substrate (results not shown) displayed a much sharper submonolayer peak, with desorption completed by 155 K. An increased surface area for C_6H_6 adsorption on the SiO_2 film as a result of surface roughness is also evidenced by a fivefold increase in the C_6H_6 exposure required for multilayer formation compared with that required on the uncoated stainless steel.

Desorption kinetic parameters can be obtained by application of the Polanyi–Wigner equation, which describes the rate of desorption, r_{des} (Refs. 43 and 44)

$$r_{des} = -\frac{dN_{ads}}{dt} = \nu_n N_{ads}^n \exp\left[-\frac{E_{des}}{RT}\right],$$

where N_{ads} is the surface coverage of adsorbate in molecules cm^{-2}, ν_n is the pre-exponential factor for a desorption process having order n, E_{des} is the desorption energy in J mol^{-1}, and T is the surface temperature in kelvin. If the pumping rate is sufficiently high, as is reasonable to assume in a UHV chamber, the mass spectrometer signal is proportional to the rate of desorption. First order desorption results in an asymmetric peak, the peak temperature of which is independent of surface concentration. As we have shown previously, this is clearly not the behavior observed for small surface concentrations in the present case.[36] Coincident trailing edges could result from second order desorption, however such a peak would be rather symmetric, which is also not in agreement with the experimentally observed peaks here. Furthermore, second order desorption generally arises as a result of an associative desorption process, and there is no reason to expect the dissociation of C_6H_6 at low temperature on a SiO_2 surface. We have therefore adopted an approach to model the experimental TPD profiles with first order desorption from a distribution of binding sites. This approach has been used successfully to describe the desorption of physisorbed CO on MgO(100),[45] and N_2 [46] and D_2 from both porous and compact ASW.[47,48] The desorption energy coverage dependence can be extracted by inverting the Polanyi–Wigner equation[46] to obtain an expression for E_{des}

$$E_{des} = -RT \ln\left[-\frac{dN_{ads}/dt}{\nu_1 N_{ads}}\right].$$

It is necessary to assume a value for the first order pre-exponential factor, ν_1, in order to perform this procedure. A value of 10^{13} s^{-1} was used, the value typically assumed for chemisorbed adsorbates, in order to account for the likely relatively strong hydrogen bonding interaction between C_6H_6 and surface hydroxyl groups. These silanol groups are expected to exist on the surface, which was not annealed to temperatures above 500 K.[49] The resulting curves were then fitted with third order exponential decay functions in order to facilitate incorporation in the desorption model. This functional form was chosen arbitrarily to obtain good agreement with the experimentally derived curve, and should be regarded as purely empirical. The curves obtained for all exposures up to 0.8 were coincident. The desorption energy variation for an exposure of 0.8 L was then incorporated into a simple first order kinetic model to generate the simulated TPD profiles shown in Fig. 4, which demonstrate good agreement with experiment. The shoulders in Fig. 4 result from variations in the experimental heating rate profiles, which were used in the simulations.

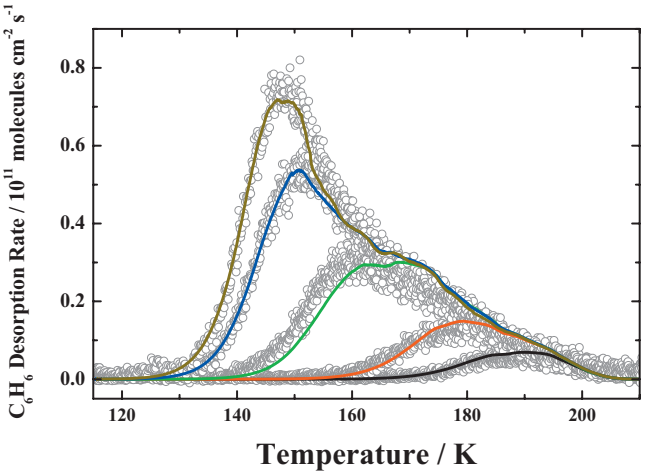

FIG. 4. Experimental (open circles) and simulated (colored lines) TPD traces for the desorption of 0.1, 0.2, 0.5, 0.7, and 0.8 L exposures of C_6H_6 from the amorphous SiO_2 substrate. The simulations incorporated the universal desorption energy curve extracted from the experimental data as described in the text. The simulations were performed with the experimental heating profiles.

The variation of desorption energy with surface concentration is shown in Fig. 5, along with the corresponding distribution of desorption energies $P(E_{des})$. The latter was obtained from the following expression:[46]

$$P(E_{des}) = -\frac{dN_{ads}}{dE_{des}}.$$

The form of this distribution clearly indicates the presence a broad distribution of desorption energies, with a significant population of high energy sites. The higher desorption energies suggest the adsorption of C_6H_6 molecules in more highly coordinated sites resulting from the roughness of the surface. It should be noted that any variation in desorption energy that results from intermolecular repulsion is also contained within the distribution as is desorption from any impurity sites on the SiO_2 surface associated with carbon contamination, which is not unrealistic for real interstellar grains. Intermolecular repulsion effects have been observed on flat, single crystal surfaces such as Pd(111).[25] On such surfaces, at low coverage, C_6H_6 molecules are adsorbed with the molecular plane parallel to the surface. For high coverages, restructuring of the monolayer occurs in which C_6H_6 molecules tilt relative to the surface, resulting in a more tightly packed layer where intermolecular repulsions become important. However, for the SiO_2 surface considered here molecules are likely to be randomly oriented on the surface as the surface is rough and presents a range of surface hydroxyl sites of random orientation to which C_6H_6 can π hydrogen bond. Intermolecular repulsion will therefore play a much smaller role in the present case.

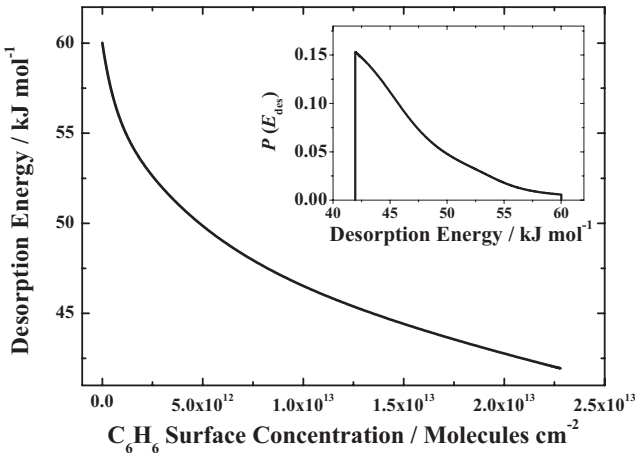

FIG. 5. The desorption energy as a function of surface concentration for the desorption of C_6H_6 from the amorphous SiO_2 substrate as obtained by direct inversion of the Polanyi–Wigner equation. A pre-exponential factor of 10^{13} s^{-1} and first order desorption were assumed. The inset shows the corresponding desorption energy distribution.

The desorption energy in the first layer is most likely to be influenced by the distribution of silanol groups on the surface. SiO_2 surfaces are generally hydroxylated as a result of exposure to atmosphere unless heated to temperatures well in excess of 500 K.[49] The silanol groups are generally considered to be important binding sites for adsorbate molecules on SiO_2 surfaces.[50] Binding is likely to be strongest on those sites where an –OH group to which the C_6H_6 molecule can hydrogen bond is present. Recent *ab initio* calculations of the surface of hydroxylated amorphous SiO_2 have revealed three distinct binding sites for H_2O on the surface depending on the coordination of the Si atom to which the OH group is attached.[51] The associated desorption energies were shown to be separated by as much as 6 kJ mol^{-1}. Large variations in binding energies for a range of molecules adsorbed on silanated SiO_2 have also been observed experimentally.[52] It is therefore reasonable to assume that hydrogen bonded C_6H_6 will behave similarly. The interaction between C_6H_6 and silanol groups has been shown through calculations to be comparable to that between C_6H_6 and H_2O clusters.[53] Island formation is likely to arise as a result of preferential binding of C_6H_6 to regions of high silanol concentration. *Ab initio* calculations of the adsorption of C_6H_6 on the different binding sites would be of great use in determining how much these effects play a role in the present case.

Desorption from the C_6H_6 films corresponding to exposures of 1 and 2 L cannot be reproduced using the same distribution of desorption energies as for lower coverages. We interpret this as being due to the formation of a second layer of C_6H_6 molecules on top of the first layer. This is also consistent with the appearance of peak B at these exposures. The presence of this additional component in the desorption profiles will then result in the apparent shift to higher desorption energy observed in the experimental TPD profiles. The sharpness of peak B suggests a narrow distribution of desorption energies in the second layer, which is to be expected as the strong site specific effects of the SiO_2 substrate are masked by the presence of the monolayer. The shape of the desorption profile for exposures between 3 and 10 L strongly suggests fractional order desorption kinetics. Such desorption kinetics could arise from the formation of islands of C_6H_6 on the saturated monolayer and or the inherent roughness of the SiO_2 surface which is also likely to be displayed by the monolayer. Both of these would result in an effective variation in film thickness across the surface, which would

lead to a fractional desorption order. It would seem more reasonable for the latter to be the dominant effect, although the formation of islands as a result of this cannot be ruled out.

For exposures above 10 L, it is apparent that desorption is in the multilayer regime, reflecting the formation of bulk C_6H_6 ice. Simple desorption kinetics that are described by a coverage independent pre-exponential factor and desorption energy can be analyzed using leading edge analysis where the initial increase in the desorption rate is considered.[44] This approach effectively casts the Polanyi–Wigner equation in the form of an Arrhenius relationship from which the activation energy for the desorption process, i.e., the desorption energy can be obtained. Suitable manipulation of the Polanyi–Wigner equation leads to

$$\ln\left[\frac{r_{\mathrm{des}}}{N_{\mathrm{ads}}^{n}}\right] = \ln[\nu_n] - \frac{E_{\mathrm{des}}}{R}\cdot\frac{1}{T}.$$

Thus a plot of $\ln(r_{\mathrm{des}}/N_{\mathrm{ads}}^{n})$ versus $(1/T)$ should yield a straight line in the leading edge region for the correct value of n. This approach was applied to the multilayer desorption profiles in order to obtain the multilayer desorption energy, characteristic of the interaction between C_6H_6 molecules in the bulk ice. A value of $n=0$ was assumed since the leading edges of the multilayer traces are highly coincident. From this analysis, a value of $E_{\mathrm{des}}=48.7\pm2$ kJ mol^{-1} was calculated for the C_6H_6 multilayers. In order obtain the pre-exponential factor a stochastic integration technique was applied using the chemical kinetics simulator (CKS) software package.[54,55] This technique has been used previously to obtain the desorption kinetics for the desorption of bulk ASW (Ref. 39) and CO from the surface of ASW.[56] A simple kinetic model was constructed with two reactions steps; (i) the desorption of C_6H_6 multilayers and (ii) the removal of C_6H_6 from the UHV chamber. In the case of (ii) the only variable is the pumping speed, which was varied to achieve best agreement with the slight pumping tail apparent on the experimental profiles. The desorption energy obtained using the leading edge analysis was used as a starting point for the analysis, with both E_{des} and ν_0 subsequently being varied in a systematic manner to achieve the best agreement with the experimental data. The simulated TPD profiles are compared with those obtained experimentally in Fig. 6 and show excellent agreement. The optimized kinetic parameters are $E_{\mathrm{des}}=48.1\pm2$ kJ mol^{-1} and $\nu_0=10^{30\pm0.5}$ molecules cm^{-2} s^{-1}. The improved agreement between different multilayer exposures demonstrates the usefulness of this technique in extracting parameters using the entire TPD peak, rather than just the higher coverage region of the leading edge, which is frequently plagued by poor signal-to-noise and experimental artifacts. The multilayer desorption energy obtained is in good agreement with the value of 48.5 ± 3 kJ mol^{-1} obtained for the highest coverage multilayer desorption of C_6H_6 from Ru(001) (Ref. 57) and the value of approximately 45 kJ mol^{-1} reported for the sublimation energy of bulk C_6H_6.[58]

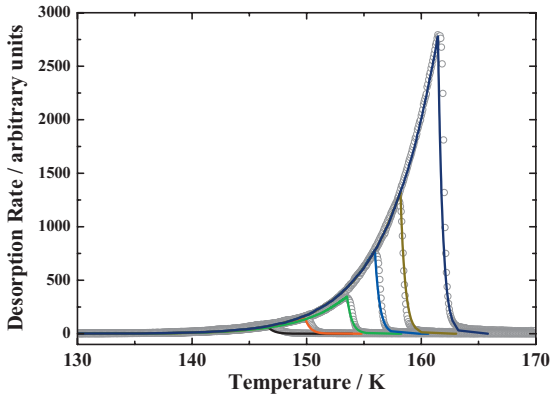

FIG. 6. Experimental (open circles) and simulated (colored lines) TPD traces for the desorption of multilayer films of C_6H_6. C_6H_6 was deposited with the substrate held at 115 K. The C_6H_6 exposures are 10, 20, 50, 100, 200, and 500 L. The kinetic parameters derived from this analysis are $E_{\mathrm{des}}=48.1\pm2$ kJ mol^{-1} and $\nu=10^{30\pm0.5}$ molecules cm^{-2} s^{-1}. A heating rate of 0.1 ± 0.02 K s^{-1} was used in all cases.

B. Adsorption of C_6H_6 on ASW

TPD traces for the desorption of sub-monolayer coverages of C_6H_6 from a thick ASW film are shown in Fig. 7. H_2O and C_6H_6 were deposited with the substrate held at 118 K. At the lowest coverages studied [see Fig. 7(a)], a single peak (peak A) is present, centered at around 130 K. As the C_6H_6 coverage is increased, this peak grows in intensity and the maximum shifts to higher temperature by a small amount. The small peak observed at around 150 K in some of the TPD traces occurs at the same temperature as the change in H_2O desorption rate, characteristic of the amor-

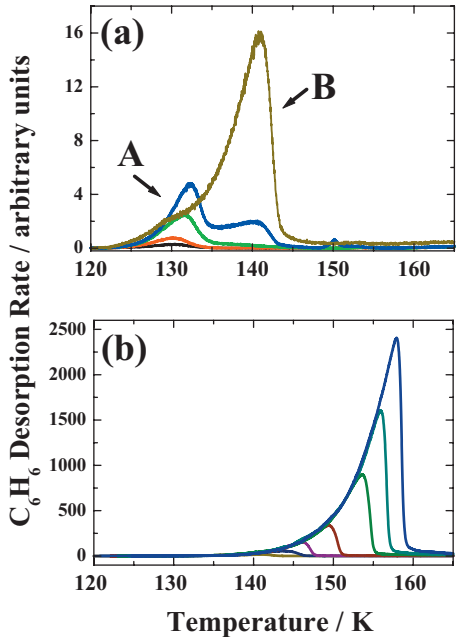

FIG. 7. Experimental TPD traces for the desorption of (a) 0.1, 0.2, 0.5, 1, and 2 L and (b) 2, 5, 10, 20, 50, 100, and 200 L exposures of C_6H_6 from compact ASW. H_2O and C_6H_6 were deposited with the substrate held at 118 K. In (a) the desorption of isolated two-dimensional C_6H_6 islands at low coverage is indicated by A, while B indicates the desorption from thee-dimensional islands at higher coverage. The desorption in (b) arises from thick multilayer films of C_6H_6. A heating rate of 0.1 ± 0.02 K s^{-1} was used in all cases.

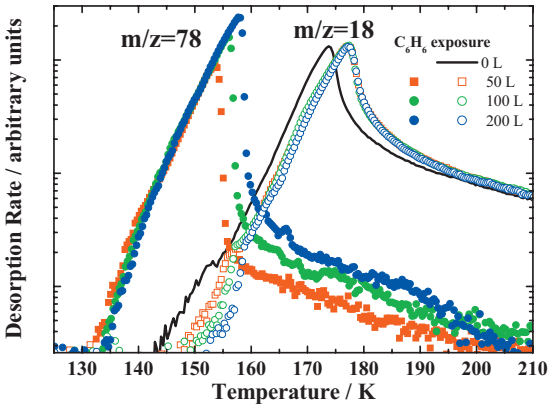

FIG. 8. Experimental TPD traces for the desorption of H_2O and C_6H_6, observed via $m/z=18$ and $m/z=78$, respectively, from varying exposures of C_6H_6 adsorbed on top of a thick layer of compact ASW. The same thickness H_2O film was used in all cases. C_6H_6 exposures of 50 (red circles), 100 (green triangles), and 200 L (blue open circles). The black line shows the desorption of H_2O from an ASW film without subsequent C_6H_6 exposure. Filled symbols indicate C_6H_6 desorption and open circles H_2O desorption. The black line shows a H_2O TPD profile obtained without C_6H_6 exposure. A heating rate of 0.1 ± 0.02 K s^{-1} was used in all cases. Note the logarithmic scale of the y-axis.

phous to crystalline phase transition of ASW. This indicates the release of a small amount of C_6H_6 that is trapped within the H_2O ice; the so-called "molecular volcano" feature as has been observed previously in the desorption of volatiles from ASW films.[32,59] We are confident that the trapping of C_6H_6 in the ASW arises as a result of displacement of C_6H_6 from surfaces within the UHV chamber during the relatively long H_2O dosing period. Even using the molecular beam, we observe a small rise in background pressure during H_2O dosing which is consistent with this observation. At around 0.5 L a shoulder appears on the high temperature side of peak A, which grows into a new peak, initially centered at around 140 K, with increasing coverage (peak B). This peak continues to grow with coverage over the entire range studied, as shown in Fig. 7(b). The peak displays coincident leading edges and a peak maximum that shifts to higher temperature with increasing coverage, indicating the formation of C_6H_6 multilayers that desorb with close to zero-order kinetics.

The non-coincidence of leading edges of peak A at low coverage suggests that C_6H_6 does not wet (i.e., spread out on) the ASW surface, resulting in the formation of three-dimensional islands,[60] which suggests that the C_6H_6–C_6H_6 interaction is stronger than that the H_2O–C_6H_6 interaction. This results in fractional order desorption kinetics at very low coverages, while the thicker of the multilayer films desorb with simple zero-order kinetics. Island formation is also evidenced by the desorption of H_2O before the completion of C_6H_6 desorption. This is shown in Fig. 8 where C_6H_6 and the associated H_2O TPD traces are shown together on a logarithmic scale. It is clear that the formation of a multilayer C_6H_6 cap inhibits the desorption of H_2O, which results in the TPD peak being shifted by 3–4 K. Once sufficient C_6H_6 to form a multilayer film has been deposited no significant peak shifting is observed, although the temperature at which H_2O desorption begins increases. It is clear that this correlates with the increasing temperature at which C_6H_6 desorption is complete for thicker films. However, in all cases the onset of H_2O desorption occurs at around 7 K before the completion of C_6H_6 desorption. When 200 L of C_6H_6 are deposited on top of the ASW, H_2O desorption commences when 100 L of C_6H_6 is remaining on the surface. Given that the desorption of 100 L of C_6H_6 from ASW displays clear zero-order kinetics it is therefore clear that multilayers of C_6H_6 are present at the commencement of H_2O desorption. This indicates that significant C_6H_6 remains on the surface and must form islands in order for H_2O desorption to be observed. This island formation, which reveals patches of the underlying ASW substrate, is characteristic of dewetting behavior.

The multilayer desorption kinetics were obtained using the combination of leading edge analysis and kinetic modeling described in Sec. III A. Zero-order kinetics were assumed, which were found to be reasonable for most of the observed desorption. The simulated TPD traces (not shown) were again in good agreement with the experimental traces, with the exception of the trailing edge region where fractional order desorption kinetics play a role. The pre-exponential factor and desorption energy obtained were $10^{29.5\pm0.5}$ molecules cm^{-2} s^{-1} and 45.8 ± 2 kJ mol^{-1}, respectively. The decrease in both ν and E_{des} compared with desorption from the SiO_2 surface is consistent with a slightly less steep profile, resulting from fractional order kinetics at low coverage. This suggests that the zero-order desorption kinetics for the bulk of the film are in agreement with those obtained for C_6H_6 adsorbed on amorphous SiO_2.

The desorption from sub-monolayer coverages of C_6H_6 on ASW displays close to first order desorption kinetics. Indeed, Bahr *et al.* also observed two peaks in the desorption of C_6H_6 from an ASW film and attributed the low temperature peak to the first order desorption of C_6H_6 from H_2O.[32] A similar desorption profile was also observed by Souda.[33] In the former case, the Redhead approach was employed to obtain a desorption energy of 39 kJ mol^{-1}. However, the use of this approach is questionable given the apparent fractional order of the desorption in this regime. The deviation from simple first order desorption kinetics was clearly observed in attempts to simulate the observed desorption traces with such desorption kinetics involving a single desorption energy. To gain further insight, the inversion technique was again employed with a desorption order of 0.9. Trial simulations with CKS indicated that this was appropriate for the overall form of the experimental profiles. The pre-exponential factor was assumed to be 5×10^{14} molecules$^{0.1}$ $cm^{-0.2}$ s^{-1}, which was obtained by considering a linear increase in ν from $\sim 10^{13}$ s^{-1} to $\sim 10^{28}$ molecules cm^{-2} s^{-1} as the desorption order is decreased from 1 to 0. The results of this analysis are shown in Fig. 9 and indicate the presence of a small distribution of desorption energies, with a value of 41 ± 0.5 kJ mol^{-1} being appropriate for much of the desorption. The significant difference in the curve obtained for a C_6H_6 exposure of 0.5 L results from the presence of the multilayer peak at high temperature. The curved shape of the profile likely results from changes in the sizes of islands during C_6H_6 desorption. The sharp spikes at the coverage extremes can be attributed to the poor signal-to-noise ratio for low desorption rates. The C_6H_6 desorption energy for

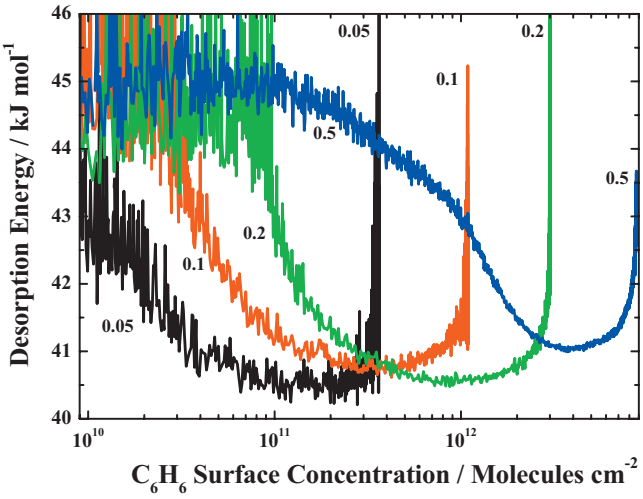

FIG. 9. The desorption energy as a function of surface concentration for the desorption of C_6H_6 from the compact ASW as obtained by direct inversion of the Polanyi–Wigner equation. A pre-exponential factor 5×10^{14} molecules$^{0.1}$ cm$^{-0.2}$ s^{-1} and a desorption order of 0.9 were assumed. The numbers indicate the C_6H_6 exposure in langmuir.

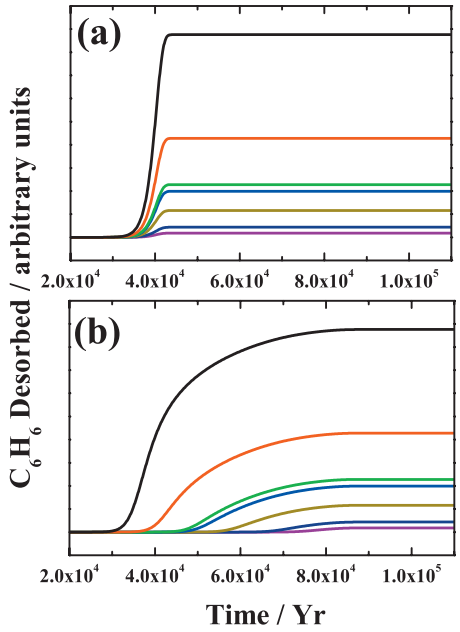

FIG. 10. Simulated desorption profiles using an astrophysical heating rate of 1 K/1000 yr. (a) shows the desorption of C_6H_6 assuming simple first order desorption kinetics and a desorption energy of 40 kJ mol^{-1}, while (b) results from the use of the experimentally obtained desorption energy distribution.

C_6H_6 adsorbed on H_2O is therefore less than that for the desorption of C_6H_6 from multilayer films, consistent with the observation of dewetting behavior. With the SiO_2 substrate there are adsorption sites which result in $SiOH-C_6H_6$ interactions that are stronger than the multilayer desorption energy. Thus, on that surface the first layer grows until the desorption energy becomes comparable to the multilayer desorption energy, at which point second layer growth commences resulting in the change in desorption kinetics observed in Fig. 1 through the appearance of peak B.

We attribute the significant differences between the submonolayer TPD profiles obtained for C_6H_6 adsorbed on amorphous SiO_2 and ASW to differences in the adsorbate-substrate binding energy. As has been discussed, in both cases, hydrogen bonding interactions between the π-system of the C_6H_6 ring and either H_2O molecules or silanol groups on the SiO_2 surface are likely to be responsible for the binding. Any differences in binding can be related to the relative acidities of the OH groups in the two surface systems. It is known through *ab initio* calculations and experiment that the deprotonation energy for surface bound silanol groups is around 1390 kJ mol^{-1}.[61] This shows that the silanol group is more acidic than H_2O, which has a deprotonation energy of approximately 1630 kJ mol^{-1} in the gas phase.[62] This is also demonstrated by the difference in solution phase pK_a values of 7 and 14 for surface silanol groups[63] and H_2O,[42] respectively. This means that the H atoms in the silanol groups will carry a partial positive charge of approximately $+0.6e$,[64] compared with those in surface H_2O molecules where the corresponding charge is $+0.4e$. As a consequence, the C_6H_6 bound to the silanol group is significantly more polarized, which in turn impacts on the interaction between the first and second C_6H_6 layers, where C_6H_6 molecules are likely to be bound edge on to those in the first layer through hydrogen bonding interactions. This explains the tendency to form a distinct second layer of C_6H_6 on amorphous SiO_2 at exposures of 1 and 2 L. The increased binding in this layer will then effectively delay the desorption of the first layer, resulting in the observed shift in the TPD profiles at these exposures. This would also suggest the formation, initially of two-dimensional islands on top of the first layer of C_6H_6 on SiO_2. In the case of the ASW substrate, the intermolecular forces between C_6H_6 molecules dominate resulting in the formation of three-dimensional islands and the observed dewetting behavior.

IV. ASTROPHYSICAL IMPLICATIONS AND CONCLUSIONS

In an astrophysical context, these results demonstrate the sensitivity of desorption kinetics to the nature of the underlying substrate. In particular, the presence of high energy binding sites will result in the return of species to the gas phase at much later times during the warm-up that occurs during cloud collapse. This is illustrated in Fig. 10 which shows the amount of C_6H_6 desorbed from the initial surface concentrations used in this work. A typical interstellar heating rate of 1 K/1000 yr (Ref. 65) was used. Figure 10(a) shows the simulation performed with a single desorption energy of 40 kJ mol^{-1}, while Fig. 10(b) employs the experimentally observed distribution of binding energies. The presence of this distribution can delay the desorption of the most strongly bound species by tens of thousands of years. The use of a single binding energy is more appropriate for the desorption of C_6H_6 from ASW. The difference in desorption behavior between the two substrates indicates that desorption is strongly dependent on whether the grains are bare, or covered by ice. The nature of the grains depends, in turn, on the local astrophysical environment. Furthermore, the binding energy for C_6H_6 on grain surfaces has been shown to be important in one mechanism for C_6H_6 formation in the ISM.[21] It is anticipated that future work will consider adsorp-

tion on H_2O ices deposited under different experimental conditions, which is known to strongly affect the surface morphology of the ice film. It is likely that a more complex desorption behavior will be observed for C_6H_6 adsorbed on H_2O deposited at low temperatures where highly porous ice is formed.

TPD has been used to study the adsorption of C_6H_6 on two surfaces of astrophysical relevance. An amorphous SiO_2 surface was used as an interstellar grain mimic, with subsequent adsorption on this surface being representative of the freeze-out of species on the cold surfaces of bare interstellar grains. Adsorption on a thick layer of ASW was used to study the interaction between C_6H_6 and grain surfaces coated with multilayers of H_2O dominated ice. The observed desorption behavior is consistent with hydrogen bonding of C_6H_6 to both surfaces through interactions with either the water molecules or silanol groups on the SiO_2 surface. Complex desorption kinetics from the latter surface indicate a broad distribution of binding sites on the rough SiO_2 surface, with the formation of a second layer of C_6H_6 molecules affecting the desorption kinetics in the high coverage regime. Adsorption on the ASW surface involves a much narrower range of binding energies, with island formation playing an important role, as is suggested by fractional order desorption kinetics and dewetting behavior observed close to the end of desorption for all C_6H_6 exposures considered.

ACKNOWLEDGMENTS

We would like to thank Dr. F. Dulieu and Dr. E. Congiu for interesting discussions regarding adsorption of amorphous surfaces. J.D.T. and M.P.C. acknowledge the support of the UK Engineering and Physical Sciences Research Council (EPSRC), Grant Nos. GR/T27044/02 and EP/D506158/1. Financial support from Heriot-Watt University for a number of upgrades to the UHV system is acknowledged. We also acknowledge the Nuffield Foundation for supporting two project students, Stephen McGurk and Sam Zawadzski, to work in our laboratory. We also thank visiting undergraduate students, Jekaterina Jeromenok and Claire Pommier, for their assistance in the laboratory.

[1] S. Suzuki, P. G. Green, R. E. Bumgarner, S. Dasgupta, W. A. Goddard III, and G. A. Blake, Science **257**, 942 (1992).
[2] S. Li, V. R. Cooper, T. Thonhauser, A. Puzder, and D. C. Langreth, J. Phys. Chem. A **112**, 9031 (2008).
[3] B. M. Cheng, J. R. Grover, and E. A. Walters, Chem. Phys. Lett. **232**, 364 (1995).
[4] M. W. Feyereisen, D. Feller, and D. A. Dixon, J. Phys. Chem. **100**, 2993 (1996).
[5] A. J. Gotch, A. W. Garrett, D. L. Severance, and T. S. Zwier, Chem. Phys. Lett. **178**, 121 (1991).
[6] A. J. Gotch and T. S. Zwier, J. Chem. Phys. **96**, 3388 (1992).
[7] A. W. Garrett and T. S. Zwier, J. Chem. Phys. **96**, 3402 (1992).
[8] R. N. Pribble and T. S. Zwier, Faraday Discuss. **97**, 229 (1994).
[9] P. Ehrenfreund and M. A. Sephton, Faraday Discuss. **133**, 277 (2006).
[10] E. Dwek, R. G. Arendt, D. J. Fixsen, T. J. Sodroski, N. Odegard, J. L. Weiland, W. T. Reach, M. G. Hauser, T. Kelsall, S. H. Moseley, R. F. Silverberg, R. A. Shafer, J. Ballester, D. Bazell, and R. Isaacman, Astrophys. J. **475**, 565 (1997).
[11] L. J. Allamandola, A. G. G. M. Tielens, and J. R. Barker, Astrophys. J., Suppl. Ser. **71**, 733 (1989).
[12] M. P. Bernstein, S. A. Sandford, L. J. Allamandola, J. S. Gillette, S. J. Clemett, and R. N. Zare, Science **283**, 1135 (1999).
[13] A. Li and J. M. Greenberg, Astron. Astrophys. **323**, 566 (1997).
[14] T. P. Snow and A. N. Witt, Astrophys. J. **468**, L65 (1996).
[15] E. L. Gibb, D. C. B. Whittet, W. A. Schutte, A. C. A. Boogert, J. E. Chiar, P. Ehrenfreund, P. A. Gerakines, J. V. Keane, A. G. G. M. Tielens, E. F. van Dishoeck, and O. Kerkhof, Astrophys. J. **536**, 347 (2000).
[16] E. A. Bergin, G. J. Melnick, J. R. Stauffer, M. L. N. Ashby, G. Chin, N. R. Erickson, P. F. Goldsmith, M. Harwit, J. E. Howe, S. C. Kleiner, D. G. Koch, D. A. Neufeld, B. M. Patten, R. Plume, R. Schieder, R. L. Snell, V. Tolls, Z. Wang, G. Winnewisser, and Y. F. Zhang, Astrophys. J. **539**, L129 (2000).
[17] M. P. Bernstein, S. A. Sandford, and L. J. Allamandola, Astrophys. J., Suppl. Ser. **161**, 53 (2005).
[18] J. D. Thrower, D. J. Burke, M. P. Collings, A. Dawes, P. D. Holtom, F. Jamme, P. Kendall, W. A. Brown, I. P. Clark, H. J. Fraser, M. R. S. McCoustra, N. J. Mason, and A. W. Parker, Astrophys. J. **673**, 1233 (2008).
[19] J. Cernicharo, A. M. Heras, A. Tielens, J. R. Pardo, F. Herpin, M. Guelin, and L. Waters, Astrophys. J. **546**, L123 (2001).
[20] R. Ruiterkamp, Z. Peeters, M. H. Moore, R. L. Hudson, and P. Ehrenfreund, Astron. Astrophys. **440**, 391 (2005).
[21] P. M. Woods and K. Willacy, Astrophys. J. **655**, L49 (2007).
[22] M. Frenklach and E. D. Feigelson, Astrophys. J. **341**, 372 (1989).
[23] U. Bardi, S. Magnanelli, and G. Rovida, Langmuir **3**, 159 (1987).
[24] S. Haq and D. A. King, J. Phys. Chem. **100**, 16957 (1996).
[25] W. T. Tysoe, R. M. Ormerod, R. M. Lambert, G. Zgrablich, and A. Ramirez-Cuesta, J. Phys. Chem. **97**, 3365 (1993).
[26] M. Xi, M. X. Yang, S. K. Jo, B. E. Bent, and P. Stevens, J. Chem. Phys. **101**, 9122 (1994).
[27] T. J. Rockey, M. C. Yang, and H. L. Dai, J. Phys. Chem. B **110**, 19973 (2006).
[28] L. H. Boulton, B. R. Clark, M. F. Coleman, and J. M. Thorp, Trans. Faraday Soc. **62**, 2928 (1966).
[29] S. K. Cutfield and J. M. Thorp, Trans. Faraday Soc. **65**, 869 (1969).
[30] B. Bilinski, J. Colloid Interface Sci. **225**, 105 (2000).
[31] S. C. Silva and J. P. Devlin, J. Phys. Chem. **98**, 10847 (1994).
[32] S. Bahr and V. Kempter, J. Chem. Phys. **127**, 074707 (2007).
[33] R. Souda, J. Phys. Chem. B **108**, 283 (2004).
[34] D. J. Oakes, Ph.D. thesis, University of East Anglia, 1994.
[35] D. J. Oakes, M. R. S. McCoustra, and M. A. Chesters, Faraday Discuss. **96**, 325 (1993).
[36] J. D. Thrower, M. P. Collings, F. J. M. Rutten, and M. R. S. McCoustra, Mon. Not. R. Astron. Soc. **394**, 1510 (2009); e-print arXiv:astro-ph/0810.4476v2.
[37] G. D. Waddill and L. L. Kesmodel, Phys. Rev. B **31**, 4940 (1985).
[38] K. P. Stevenson, G. A. Kimmel, Z. Dohnálek, R. S. Smith, and B. D. Kay, Science **283**, 1505 (1999).
[39] H. J. Fraser, M. P. Collings, M. R. S. McCoustra, and D. A. Williams, Mon. Not. R. Astron. Soc. **327**, 1165 (2001).
[40] A. S. Bolina, A. J. Wolff, and W. A. Brown, J. Phys. Chem. B **109**, 16836 (2005).
[41] G. Strazzulla and G. A. Baratta, Astron. Astrophys. **241**, 310 (1991).
[42] P. W. Atkins, *Physical Chemistry* (Oxford University Press, Oxford, 1998).
[43] D. A. King, Surf. Sci. **47**, 384 (1975).
[44] A. M. de Jong and J. W. Niemantsverdriet, Surf. Sci. **233**, 355 (1990).
[45] Z. Dohnálek, G. A. Kimmel, S. A. Joyce, P. Ayotte, R. S. Smith, and B. D. Kay, J. Phys. Chem. B **105**, 3747 (2001).
[46] T. Zubkov, R. S. Smith, T. R. Engstrom, and B. D. Kay, J. Chem. Phys. **127**, 184707 (2007).
[47] L. Amiaud, F. Dulieu, J. H. Fillion, A. Momeni, and J. L. Lemaire, J. Chem. Phys. **127**, 144709 (2007).
[48] L. Hornekær, A. Baurichter, V. V. Petrunin, A. C. Luntz, B. D. Kay, and A. Al-Halabi, J. Chem. Phys. **122**, 124701 (2005).
[49] I. Gillis-D'Hamers, I. C. Cornelissens, K. C. Vrancken, P. Van Der Voort, and E. F. Vansant, J. Chem. Soc., Faraday Trans. **88**, 723 (1992).
[50] R. K. Iler, *The Chemistry of Silica* (Wiley, New York, 1979).
[51] F. Tielens, C. Gervais, J. F. Lambert, F. Mauri, and D. Costa, Chem. Mater. **20**, 3336 (2008).
[52] B. Fubini, V. Bolis, A. Cavenago, E. Garrone, and P. Ugliengo, Langmuir **9**, 2712 (1993).
[53] T. Suzuki, H. Tamon, and M. Okazaki, Chem. Lett. **23**, 2151 (1994).

[54] Chemical Kinetics Simulator (CKS), version 1.0, IBM Almaden Research Center, 650 Harry Road, Mailstop ZWX1D1, San Jose, CA, USA. Further information may be obtained from the CKS website at http://www.almaden.ibm.com/st/msim/ckspage.html.
[55] F. A. Houle and W. D. Hinsberg, Surf. Sci. **338**, 329 (1995).
[56] M. P. Collings, J. W. Dever, H. J. Fraser, and M. R. S. McCoustra, Astrophys. Space Sci. **285**, 633 (2003).
[57] P. Jakob and D. Menzel, Surf. Sci. **220**, 70 (1989).
[58] J. S. Chickos and W. E. Acree, J. Phys. Chem. Ref. Data **31**, 537 (2002).
[59] R. S. Smith, C. Huang, E. K. L. Wong, and B. D. Kay, Phys. Rev. Lett. **79**, 909 (1997).
[60] K. W. Kolasinski, *Surface Science: Foundations of Catalysis and Nanoscience* (Wiley, New York, 2002).
[61] J. Sauer and J.-R. Hill, Chem. Phys. Lett. **218**, 333 (1994).
[62] D. Heidrich, D. Volkmann, and B. Zurawski, Chem. Phys. Lett. **80**, 60 (1981).
[63] M. L. Hair and W. Hertl, J. Phys. Chem. **74**, 91 (1970).
[64] A. Pedone, G. Malavasi, M. C. Menziani, U. Segre, F. Musso, M. Corno, B. Civalleri, and P. Ugliengo, Chem. Mater. **20**, 2522 (2008).
[65] S. Viti, M. P. Collings, J. W. Dever, M. R. S. McCoustra, and D. A. Williams, Mon. Not. R. Astron. Soc. **354**, 1141 (2004).